JBMR Plus, 2026, **10**, ziaf178
https://doi.org/10.1093/jbmrpl/ziaf178
Advance access publication: November 7, 2025
Research Article

Estrogen signaling in PDGFRα+ cells positively regulates cortical bone metabolism via IGFBP5 in female mice

Aoi Ikedo[1], Reina Aoki[2], Hiroshi Sakai[1,3], Noritaka Saeki[1,4], Yuta Yanagihara[1], Jonathan Moody[5], Miki Kojima[5], Tsukasa Kouno[5], Yoshinari Ando[5], Kazunori Hino[6], Tomofumi Kinoshita[6], Piero Carninci[5,7], Jay W. Shin[5,8,9], Chung-Chau Hon[5], Akiyoshi Uezumi[10], Yoshiaki Kamei[2], Yuuki Imai[1,3,*]

[1]Division of Integrative Pathophysiology, Proteo-Science Center, PIAS, Ehime University, Toon 791-0295, Japan
[2]Department of Hepato-Biliary-Pancreatic Surgery and Breast Surgery, Ehime University Graduate School of Medicine, Toon 791-0295, Japan
[3]Department of Pathophysiology, Ehime University Graduate School of Medicine, Toon 791-0295, Japan
[4]Division of Medical Research Support, Advanced Research Support Center, Ehime University, Toon 791-0295, Japan
[5]Laboratory for Regulatory Genomics, RIKEN Center for Integrative Medical Sciences, Yokohama 230-0045, Japan
[6]Department of Orthopaedic Surgery, Ehime University Graduate School of Medicine, Toon 791-0295, Japan
[7]Human Technopole, 20157 Milan, Italy
[8]Genome Institute of Singapore (GIS), Agency for Science, Technology and Research (A∗STAR), Singapore 138672
[9]Department of Biochemistry, Yong Loo Lin School of Medicine, National University of Singapore, Singapore 117597
[10]Divison of Cell Heterogeneity, Medical Research Center for High Depth Omics, Medical Institute of Bioregulation, Kyushu University, Fukuoka 812-0054, Japan

*Corresponding author: Yuuki Imai, Division of Integrative Pathophysiology, Proteo-Science Center, PIAS, Ehime University, Shitsukawa, Toon, Ehime 791-0295, Japan (y-imai@m.ehime-u.ac.jp).

Abstract

The prevalence of both osteoporosis and sarcopenia increases with age and about 60% of elderly sarcopenia patients also develop osteoporosis. However, the co-occurrence of osteoporosis and sarcopenia remains unclear. We performed single-cell 5′ RNA-seq on human skeletal muscle tissues and investigated the enrichment of heritability for musculoskeletal traits in cell type specific cis-regulatory regions. We found the fibroblast-specific cis-regulatory regions are highly enriched in the heritability of bone mineral density (BMD). Using genome-wide association study, we identified estrogen receptor α (*ESR1*) as a common transcription factor that correlated with both BMD and lean mass. We hypothesized that deficiency of estrogen signaling in fibroblast may attenuate musculoskeletal homeostasis. Therefore, we generated mice lacking *Esr1* in PDGFRα (a fibroblast marker)+cells ($Esr1^{\Delta Pα}$). Although muscle mass and grip strength were not different between groups, distal femoral BMD and cortical thickness were significantly lower in $Esr1^{\Delta Pα}$ compared to control. Bone histomorphometry showed that cortical bone in $Esr1^{\Delta Pα}$ exhibited a high turnover bone phenotype. Bulk RNA-seq using PDGFRα+ cells revealed that insulin-like growth factor-binding protein 5 (*Igfbp5*) expression was significantly higher in $Esr1^{\Delta Pα}$ compared to control. Furthermore, serum IGFBP5 level was significantly higher in $Esr1^{\Delta Pα}$. IGFBP5 treatment in vitro significantly suppressed osteoblast differentiation and facilitated osteoclast differentiation. These results suggest that estrogen signaling in PDGFRα+ cells suppresses *Igfbp5* expression, then maintains bone mass, indicating that estrogen signaling in PDGFRα+ cells plays a significant role in bone metabolism.

Keywords: human cell atlas, estrogen, PDGFRα+ cells, Igfbp5; bone metabolism

Lay Summary

Decreases in the amount of bone and muscle often occur together in older adults. To better understand the relationship between the decline in these tissues, we examined gene expression in individual cells found in human muscle and related that to large population studies of genes correlated with both bone and muscle mass. This led us to use mice to study the role of a receptor for estrogen (Esr1) in fibroblasts, a cell type found in both muscle and bone. We identified IGFBP5, a factor expressed in fibroblasts and found in blood, that may explain some of the bone changes in females.

Received: April 5, 2025. **Revised:** October 30, 2025. **Accepted:** November 3, 2025

Graphical Abstract

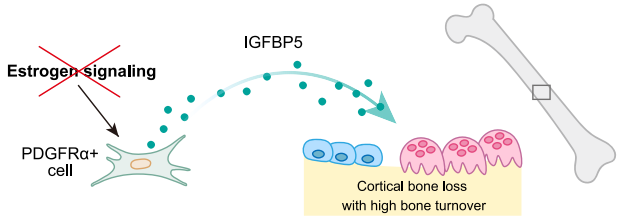

Introduction

Independent mobility is necessary to extend the healthy life expectancy of older people. Treatment of osteoporosis and sarcopenia in patients with reduced mobility can improve independent mobility in older people. The prevalence of both osteoporosis and sarcopenia increases with age and about 60% of elderly Japanese sarcopenia patients also develop osteoporosis.[1] Sarcopenia, an age-related atrophy of skeletal muscle, which increases the risk of falls and fragility fractures associated with osteoporosis, reduces activities of daily living in the elderly. In fact, the coexistence of osteoporosis and sarcopenia has been considered recently as a syndrome termed "osteosarcopenia." The prevalence of osteosarcopenia in community-dwelling adults ≥65 yr of age ranges between 5% and 37%, with the highest rates observed in those with fractures.[2]

Estrogen deficiency in postmenopausal osteoporosis can induce bone loss by disrupting estrogen/estrogen receptor (ER) signaling, which is important for various physiological functions. This signaling dysfunction alters the maintenance of osteoclastic life span,[3] maintenance of osteoblast/osteocyte functions by Wnt signaling,[4–6] inhibition of inflammatory cytokine production,[7] and negative feedback regulation of follicle stimulation hormone (FSH) secretion.[8] However, the pathogenesis of postmenopausal sarcopenia remains unclear. It has been reported that rate of fat gain doubles, and lean mass decreases during the menopause transition, and these gains and losses of fat and muscle mass continue until 2 yr after the final menstrual period.[9] In addition, appendicular lean mass and grip strength, a generalized surrogate for muscle strength, were significantly decreased in postmenopausal women compared to premenopausal women.[10] In animal studies, mice with ovariectomy (OVX) exhibited not only muscle atrophy and low muscle force, but also shifted fiber types toward faster myosin heavy chain isoforms compared to sham mice.[11] Furthermore, according to a study of muscle (mKO)-or satellite cell (scKO)-specific ER β (ERβ)-KO mice, young female mKO mice had reduced fast-type dominant muscle mass, while female scKO mice displayed compromised muscle regeneration after acute muscle injury.[12] These findings suggested that estrogen regulates muscle mass and function.

In this study, analysis using single-cell RNA-seq (scRNA-seq) of human skeletal muscle revealed that the gene expression profile of fibroblasts was correlated significantly with related genes of BMD as well as muscle strength. Furthermore, based on the genome-wide association study (GWAS) database, estrogen receptor α (*ESR1*) is a common gene correlated with both muscle and bone mass. Therefore, we generated mice lacking *Esr1* in platelet-derived growth factor receptor-α (PDGFRα)+ cells, a fibroblast, and performed bone and skeletal muscle phenotypic analyses.

Materials and methods

Human subjects

All human samples examined in this study were either exempted materials or obtained with informed consent and were covered under the research protocols at Ehime University Hospital IRB (1812005). Written informed consent was obtained from all participants for sample collection, data acquisition, usage, and publication.

Sample preparation for scRNA-seq

As registered in bioRxiv,[13] skeletal muscle ($n = 2$) and articular cartilage ($n = 2$) biopsies were obtained from the muscle tissues surrounding the knee joint and undamaged cartilage tissues of the knee joint respectively from patients with osteoarthritis ($n = 2$) during artificial joint surgery. Mononuclear cells were isolated from muscle biopsies using a method described[14] with minor modifications. Briefly, muscle biopsies were minced in PBS on ice and digested using 800 U/mL collagenase type 2 in F10 medium supplemented with 10% horse serum and antibiotic–antimycotic for 60 min. An additional 30-min digestion was performed using 1000 U/mL collagenase type 2 and 11 U/mL dispase. The supernatants were filtered through a cell strainer (Falcon, Cat# 352340) to remove debris and then centrifuged (500 × *g* for 5 min) to obtain a cell suspension. Chondrocytes were isolated from articular cartilage by slicing the dissected tissue into 2-3 mm pieces, followed by incubation with 0.1% trypsin for 30 min at 37 °C. After washing, the tissues were digested with 1 mg/mL collagenase type 2 for 2-3 h at 37 °C with shaking. The resulting solution was centrifuged at 700 rpm for 5 min, and the sediment was subjected to a second digestion with fresh 1 mg/mL collagenase type 2 for 2-3 h at 37 °C with shaking before filtration through a 40 μm cell strainer to obtain chondrocytes. Both types of cells were cryopreserved in cell freezing media respectively.

scRNA-seq experiment

As registered in bioRxiv,[13] cryovials of cell samples were thawed in a 37 °C water bath for 2 min until no visible ice crystals were seen, and further thawed using prewarmed thawing media (DMEM + 10% FBS). The cell samples were transferred to 2-mL tubes, centrifuged at 500 × *g* for 5 min at room temperature, and the supernatant was removed. Cells were sequentially diluted by incremental 1:1 volume additions of thawing media 5 times with a ∼1 min wait between additions. Cell samples were centrifuged at 500 × *g* for 5 min at room temperature and the supernatant removed. Cell number

and viability were measured using a Countess II Automated Cell Counter (Thermo Fisher). Cells were resuspended to 1.0×10^6 cells/mL in PBS + 0.1% bovine serum albumin. About 10000 cells were loaded to the Chromium Controller (10x Genomics) and library preparation was performed using the Chromium Single Cell 5′ Library & Gel Bead kit v1 (10x Genomics) according to the manufacturer's instructions. The size profiles of the libraries were examined using Bioanalyzer (Agilent) and quantified by KAPA Library Quantification Kits (Kapa Biosystems). One library was constructed for each of the 4 biopsies. Libraries were sequenced on HiSeq2500 High-Output (Illumina) as 50 bp paired-end reads.

scRNA-seq data alignment, filtering, doublet removal, and processing

As registered in bioRxiv,[13] Fastq from the scRNAseq libraries of the samples were aligned to hg38 using *Cell Ranger v3.1.0*. Gene expression counts were corrected for ambient RNA using cellbender[15] v0.2.0, using 0.6× and 2.5× cellranger identified cell counts as expected-cells and total-droplets included. Doublet removal was performed with *scrublet*,[16] and cells with fewer than 500 unique molecular identifiers (umi), 300 genes, or more than 10% mitochondrial UMI were removed. Variable genes were identified using *scanpy.pp.highly_variable_genes* flavour = seurat_v3, batch_key = project, span = 0.5. Unique molecular identifiers counts of genes were normalized to 1×10^4 per cell and log transformed. Twenty principal components were used for *bbknn*[17] for batch correction. Batched corrected nearest-neighbors graphs were used in UMAP projection and Leiden clustering.

Cell annotation and clustering

Cells were initially annotated using *CellO v1.2.0*[18] and manually revised after clustering. Cells were clustered using the Leiden clustering algorithm implemented in the *FindClusters* of *Seurat v3*[19] at various resolutions. An optimal clustering resolution was manually chosen based on biological interpretations of the initial cell annotations, resulting in 7 visually distinct clusters on UMAP annotated as 7 broad cell types.

Identification of cell-type specific transcribed cis-regulatory elements

As registered in bioRxiv,[13] to define and annotate transcribed cis-regulatory elements (tCREs), we used SCAFE v1.0.0 as described.[20] Briefly, the single nucleotide resolution 5′ Cap transcriptional start sites (CTSS) signals were extracted from the alignment bam files generated from cellranger and the CTSS signals from the 4 libraries were aggregated. The aggregated CTSS signals were clustered in *SCAFE* using default parameters. Transcriptional start sites clusters that are potentially strand invasion artifacts[20] were removed and the remaining TSS clusters were further filtered using a logistic regression classifier implemented in *SCAFE*. A default logistic probability cutoff of 0.5 was used. The filtered TSS clusters were then merged by extending 400 nt upstream and 100 nt downstream. These merged TSS clusters were defined as tCREs. The expression of tCREs in single cells was quantified by counting the number of UMI within the tCREs using *SCAFE* and then normalized in *Seurat* to 1×10^4 per cell and log transformed. Cell type-enriched expression of tCREs was quantified using the *FindMarkers* function in *Seurat* min.pct = 0, return.thresh = Inf, logfc.threshold = 0, min.cells.group = 0.

Enrichment of trait heritability

As registered in bioRxiv,[13] summary statistics of GWAS of musculoskeletal and related traits in the UK Biobank were downloaded from "UKB SNP-Heritability Browser" on July 13, 2021 at https://nealelab.github.io/UKBB_ldsc/h2_browser.html, including BMD, heel BUA, ankle spacing width, hand grip strength, height, forearm fracture, and osteoarthritis. Genome-wide association study summary statistics for rheumatoid arthritis were downloaded from https://alkesgroup.broadinstitute.org/sumstats_formatted/ as a non-musculoskeletal trait control (Table S1). To quantify the enrichment of the heritability of these traits in cell type-enriched tCREs, we used Linkage Disequilibrium Score Regression for Specifically Expressed Genes (LDSC-SEG) with the 53 annotations baseline-LD model v1.2.[21] Briefly, for each of the 7 cell types, including chondrocytes, endothelial cells, myoblasts, smooth muscle cells, fibroblasts, monocytes/macrophages, and T cells, the top 20% cell type-enriched tCREs (ranked by the *p*-value from *FindMarkers* in *Seurat*) were used as the "foreground" and the rest of the tCREs were used as the "background". The "foreground" tCRE regions were compared against the "background" tCRE regions by running *ldsc.py* –h2-cts, yielding a *p*-value and a regression coefficient for each trait-cell type pair. The heritability of a trait is defined as significantly enriched in a cell type when the *p*-value is smaller than the Bonferroni corrected multiple hypothesis testing threshold for 7 cell types, that is, 0.05/7 = 0.00714.

Motif analysis

Motif enrichment analysis of cell type-enriched tCREs was performed with HOMER (v5.1)[22] findMotifsGenome with -size 100 -mask options and tCREs were annotated to Human hg 38 genes using annotatePeaks (-size 100 -mask) from cell type-enriched tCRE files (Table S2).

Animals

PDGFRα-CreERT mice[23] were obtained from the Jackson Laboratories (Strain #: 018280). *Esr1*$^{flox/flox}$ mice were kindly provided by Prof. Chambon.[24] *PDGFRα-CreERT* male mice were crossed with *Esr1*$^{flox/flox}$ female mice to generate *PDGFRα-CreERT;Esr1*$^{flox/flox}$ mice. Female littermates with the *PDGFRα-CreERT;Esr1*$^{+/+}$, *PDGFRα-CreERT;Esr1*$^{flox/+}$, or *Esr1*$^{flox/flox}$ genotype were used as control mice. All mice were housed in a specific pathogen-free facility under climate-controlled conditions and a 12-h light/dark cycle and were provided water and a standard diet (MF, Oriental Yeast Co. Ltd.) ad libitum. In both control and mutant mice, 100 μL of 20 mg/mL tamoxifen (TMX, Sigma-Aldrich, Cat# T5648), dissolved in corn oil (Sigma-Aldrich, Cat# C8267), was injected intraperitoneally for 5 consecutive days at 11 wk of age. All animal experiments were approved by the Animal Experiment Committee of Ehime University (Approval No. 37A1-1·16) and were conducted in full compliance with the Guidelines for Animal Experiments at Ehime University.

Grip strength

The grip strength of the forelimb was measured using a strain gauge (Melquest, Cat# GPM-100B) before sacrifice

of each mouse. The maximum force was determined after 10 measurements and reported as the grip strength of each mouse.

RNA isolation and quantitative real-time PCR

Total RNA was isolated from freshly sorted skeletal muscle PDGFRα+ cells in mice and cultured MC3T3-E1 cells using the RNeasy Plus Micro Kit (Qiagen, Cat# 74034) or the ISOGEN (319-90211, Nippon Gene Co., Ltd.) with EconoSpin for RNA (EP-21201, Ajinomoto Bio-Pharma) according to the manufacturer's instructions. Subsequently, reverse transcription was carried out using PrimeScript (Takara, Cat# RR036A) to synthesize cDNA from the extracted total RNA. Quantitative PCR (qPCR) was performed on technical duplicate samples using TB Green Premix Ex Taq II (Takara, Cat# RR820S) and the Thermal Cycler Dice (Takara, Cat# TP850). The expression levels of the target genes were normalized to the expression of *Rpl13a*. Detailed primer sequences are provided in Table S3.

Radiological examination

Animal samples were fixed in 4% paraformaldehyde phosphate buffer solution (PFA) overnight at 4 °C. The areal BMD of the isolated tibiae and femora was measured by dual-energy x-ray absorptiometry (DXA) using a bone mineral analyzer (DCS-600EX, ALOKA). Micro-CT (μCT) scanning of the femora was performed according to the manufacturer's instructions using a Scanco Medical μCT35 System (SCANCO Medical) with an isotropic voxel size of 6 μm. We defined the regions of interest (ROI) as 300 slices starting distal to the distal growth plate in the femur. These images were used for 3D reconstruction and analysis. Structural parameters (3D) included cortical structure [bone area per total area (BA/TA), BMD, cortical thickness (Ct.Th), periosteal perimeter, and endosteal perimeter], and trabecular structure [bone volume per total volume (BV/TV), trabecular thickness (Tb.Th), BMD, trabecular space (Tb.Sp), trabecular number (Tb.N), and connective density (Conn-Dens.)] according to established guidelines.

Osmium staining

Osmium staining was performed to evaluate marrow fat using the left tibia following a method previously described.[25] Briefly, tibiae were harvested, fixed in 4% PFA overnight, and then immersed in 0.1 M EDTA (pH 7.3) for 2 wk for decalcification. The decalcified tibiae were immersed in a 1:1 mixture of 5% potassium dichromate (Wako, Cat# 162-03652) and 2% osmium tetroxide (Polysciences, Inc., Cat# 23310-10) for 48 h and stained. The stained tibiae were scanned using μCT to evaluate marrow fat volume.

Histology and histomorphometry

For bone histomorphometry, the mice were double labeled with an intraperitoneal injection of 15 mg/kg of calcein (Sigma, Cat# C-0875) 5 and 2 d before sacrifice. Femora were removed from each mouse and fixed with 4% PFA. After μCT analysis, femora were embedded with methylmethacrylate after dehydration, and the plastic sections were cut using a standard microtome (LEICA) into 6 μm to observe calcein labeling, TRAP staining, and toluidine blue staining. The ROI was 250 × 800 mm of cortical bone distal to the distal femoral growth plate. Each section was photographed using a cellSense Ver. 1.3 (OLYMPUS) and analyzed using OsteoMeasure V3.3.0.1 (OsteoMetrics, Inc.).

Isolation of mesenchymal progenitors from skeletal muscle

Mononuclear cells were isolated from muscle tissue in mice following a method previously described[14] with minor adjustments. Briefly, muscles were minced in PBS on ice and digested using 800 U/mL collagenase type 2 (Worthington, Cat# LS004177) in F10 medium (Gibco, Cat# 11550-043) supplemented with 10% horse serum (Gibco, Cat# 26050-088) and antibiotic-antimycotic (Gibco, Cat# 15240-062) for 60 min. Subsequently, an additional digestion step was performed using 1000 U/mL collagenase type 2 and 11 U/mL dispase (Gibco, Cat# 17105-041) for 30 min. The resulting supernatants were filtered through a 40 μm cell strainer (Falcon, Cat# 352340) to remove debris and then centrifuged to obtain a cell suspension. The following antibodies were used for fluorescence-activated cell sorting (FACS): FITC anti-CD31 (BioLegend, Cat# 102406; RRID: AB_312901; 1/100), FITC anti-CD45 (BioLegend, Cat# 103108, RRID: AB_312973; 1/100), PE anti-VCAM1 (Thermo Fisher Scientific, Cat# 12-1061-82, RRID: AB_2572573; 1/100), and APC anti-PDGFRα (R&D Systems, Cat# FAB1062A, RRID: AB_3073817; 1/30). Fluorescence-activated cell sorting was performed using the BD FACSAria II (BD Biosciences), and data were analyzed using FlowJo v10.1r7 (BD Life Sciences).

Bulk RNA-seq and data analysis

A total of 30000 PDGFRα+ cells were isolated from skeletal muscles. About 4000 to 8000 of PDGFRα+ cells were isolated from around the growth plate in tibial and femoral bone. High-quality total RNA was obtained using the RNeasy Plus Micro Kit (Qiagen, Cat# 74034) and verified using an Agilent 2100 Bioanalyzer. RNA-seq was performed by Kazusa DNA Research Institute using an Illumina NextSeq 500 with a read configuration of 75 bp for single reads; 1 million reads were generated per sample. Obtained FASTQ files were analyzed by QIAGEN CLC Genomics Workbench. Data were registered in GEO with the accession number GSE279051. Enrichment analysis was conducted by Metascape.[26]

Serum analysis

Blood samples were collected from the heart when mice were sacrificed. Blood samples were centrifuged at 3000 × *g* at 4 °C for 10 min, and separated serum samples were frozen and stored at −80 °C until analysis. Serum IGFBP5 concentration was measured using DuoSet Mouse IGFBP-5 (R&D systems, Cat# DY578) and DuoSet Ancillary Reagent Kit (R&D systems, Cat# DY009B).

Cell culture

The MC3-T3 E1 cell line was seeded with 1×10^5 cells in a 48 well plate containing growth medium (α-MEM (Gibco, Cat# 12571-063) with 10% FBS and 1% antibiotic-antimycotic solution) and cultured at 37 °C. The cells were left overnight and then switched to differentiation medium (α-MEM containing 10% FBS, 10 mM β-glycerophosphate, and 50 μg/mL ascorbic acid, 1% antibiotic-antimycotic solution). The differentiation medium was replaced every 2 d. After 7 d of culture, ALP staining (Wako, Cat# 294-67001) was used to measure differentiation capacity. Quantitation of the stained area was

performed using Fiji (v2.14.0) (https://imagej.net/Fiji). The RAW264 cell line was seeded with 0.75×10^3 cells in a 96-well plate containing α-MEM (Gibco, Cat# 12571-063) with 10% FBS (CORNING, Cat# 35-010-CV), nonessential amino acids (NEAA) (Gibco, Cat# 11140-050) and 1% antibiotic-antimycotic solution. After leaving them overnight, 50 ng/mL soluble RANKL (Oriental Yeast Co. Ltd., Cat# 47197900) was added to the medium. The medium was replaced every 2 d. After 4 d of culture, TRAP staining (Wako, Cat# 294-67001) was used to measure the number of multi-nucleated osteoclasts. The MC3-T3 E1 cell line and RAW264 cell line were cultured with or without recombinant Mouse IGFBP-5 (BioLegend, Cat# 751204).

Isolation of calvarial pre-osteoblasts and osteoblastic differentiation with conditioned medium

Calvaria from individual postnatal 2- to 3-day-old mice were carefully excised excluding soft tissue using sterile techniques. The calvaria was digested in 1 mg/mL Collagenase A (Cat# 10103578001, Roche) in sterile PBS at 37 °C for 30 min with constant shaking. The calvaria was washed in PBS and thoroughly minced with scissors. Then the minced calvaria was digested again in 1 mg/mL Collagenase A in PBS at 37 °C for 60 min with constant shaking. The digested calvaria was centrifuged at $400 \times g$ for 5 min and reconstructed in a-MEM containing 10% FBS and 1% antibiotic/antimycotic and then cultured until confluence after filtration. After confluency, cells seeded with 1×10^5 cells in a 48-well plate containing growth medium. The cells were left overnight and then switched to mix of growth medium and conditioned medium of PDGFRα+ cells (1:1) with 10 mM β-glycerophosphate, and 50 μg/mL ascorbic acid. After 7 d of culture, ALP staining was performed. The conditioned medium was collected from cultured muscle PDGFRα+ cells with a-MEM containing 10% FBS and 1% antibiotic/antimycotic at day 1 and 2, respectively.

Statistical analysis

The data are presented as means ± SD using nonparametric Mann–Whitney U test. Outliers were excluded using the Smirnov–Grubbs test. All statistical analyses were performed using GraphPad Prism Version 10.0.2 (GraphPad Software Inc.) and Microsoft Excel. p-values less than .05 were considered significant.

Results

Fibroblasts gene expression from human skeletal muscle correlated with BMD and muscle strength related genes

To investigate association between joint including cartilage and skeletal muscle and musculoskeletal traits, we performed combined analysis of scRNA-seq data and GWAS data. We collected muscle ($n = 2$) and cartilage biopsies ($n = 2$) from an undamaged area of the knee in osteoarthritis patients and performed scRNA-seq analysis (Figure 1A). In total, 17 524 cells were profiled, and 7 distinct cell clusters were identified, including chondrocytes, endothelial cells, myoblasts, smooth muscle cells, fibroblasts, monocytes/macrophages, and T cells (Figure 1B). Of these, the chondrocyte clusters were derived from cartilage biopsies, and the other 6 clusters were derived from muscle biopsies. Next, we investigated associations between these cell types and musculoskeletal traits from a genetic perspective. Trait-associated variants are enriched in cis-regulatory elements (CREs).[27] CREs regulate gene expression by recruiting transcription factors and RNA polymerase II to start the transcription of capped-RNA[28] at both promoter and enhancer sites.[29] Sequencing the 5′-end of RNAs identifies TSS and thus tCREs. Thus, we defined tCREs in these cell types based on the TSS signals extracted from the single-cell RNA-seq data.[20] In total, 51 224 tCREs were defined, with 33 894 of them located within 500 nt to annotated promoters in GENCODEv32 and the rest of them ($n = 17\,330$) representing potential enhancers (Table S4). We then quantified the enriched expression of tCREs in each of the 7 cell types (Table S2) and examined the enrichment of musculoskeletal trait heritability (Table S1, from GWAS in the UK Biobank Axiom array,[30] Table S5) in the cell type-enriched tCREs using the LDSC-SEG.[21] Fibroblast-enriched tCREs were enriched significantly for the heritability of BMD, heel BUA, ankle spacing width, hand grip strength and height (p-value < .0071, adjusted threshold, Figure 1C). These results imply the involvement of fibroblast-enriched genes in skeletal development and maintenance, as well as muscle strength. As a control, fibroblast-enriched tCREs were not enriched in the heritability of the immunological trait rheumatoid arthritis while T-cell-enriched tCREs were (Figure 1C), suggesting that the observed associations between fibroblasts and musculoskeletal traits are specific.

ESR1 was identified as the common gene regulating both bone and muscle mass

To identify regulatory common genes between bone and skeletal muscle, we explored gene-level associations for lumbar spine (LS) BMD and total body lean mass using the Musculoskeletal Knowledge Portal (http://mskkp.org/). Musculoskeletal Knowledge Portal is a public database, which enables browsing, searching, and analysis of human genetic and genomic information linked to musculoskeletal traits and diseases. We found 943 genes associated with LS BMD and 944 genes associated with total body lean mass. Then, we extracted 56 genes common between the 2 gene sets. When we focused on transcriptional factors among these, *ESR1* was found as the top-ranked gene of the transcription factor (Figure 1D). Furthermore, we performed Motif analysis using cell type-enriched tCREs data. As a result, JunB and AP-1 site were found within the top 15 of fibroblasts enriched tCREs (Figure S1). The role of ER action at the AP-1 site has been confirmed by several studies. The binding of Jun and Fos to the AP-1 site is needed for ER action, and ER appears to increase the intrinsic transcriptional activity of Jun/Fos when bound to the site.[31] Thus, we hypothesized that estrogen signaling in fibroblasts may regulate musculoskeletal homeostasis.

Esr1$^{\Delta Pα}$ female mice had less bone mass in the distal femur, but no change in muscle or fat mass

Pdgfra is known to be expressed broadly in mesenchymal cells including fibroblasts.[32] PDGFRα+ cells exist in bone tissue as a skeletal stem cell,[33] osteoblast lineage cells,[34] and septoclasts.[35] Also, PDGFRα+ cells localized in the interstitial spaces of skeletal muscle are known as mesenchymal progenitors.[36] These cells were identified as the major contributor to ectopic adipose formation in muscles and

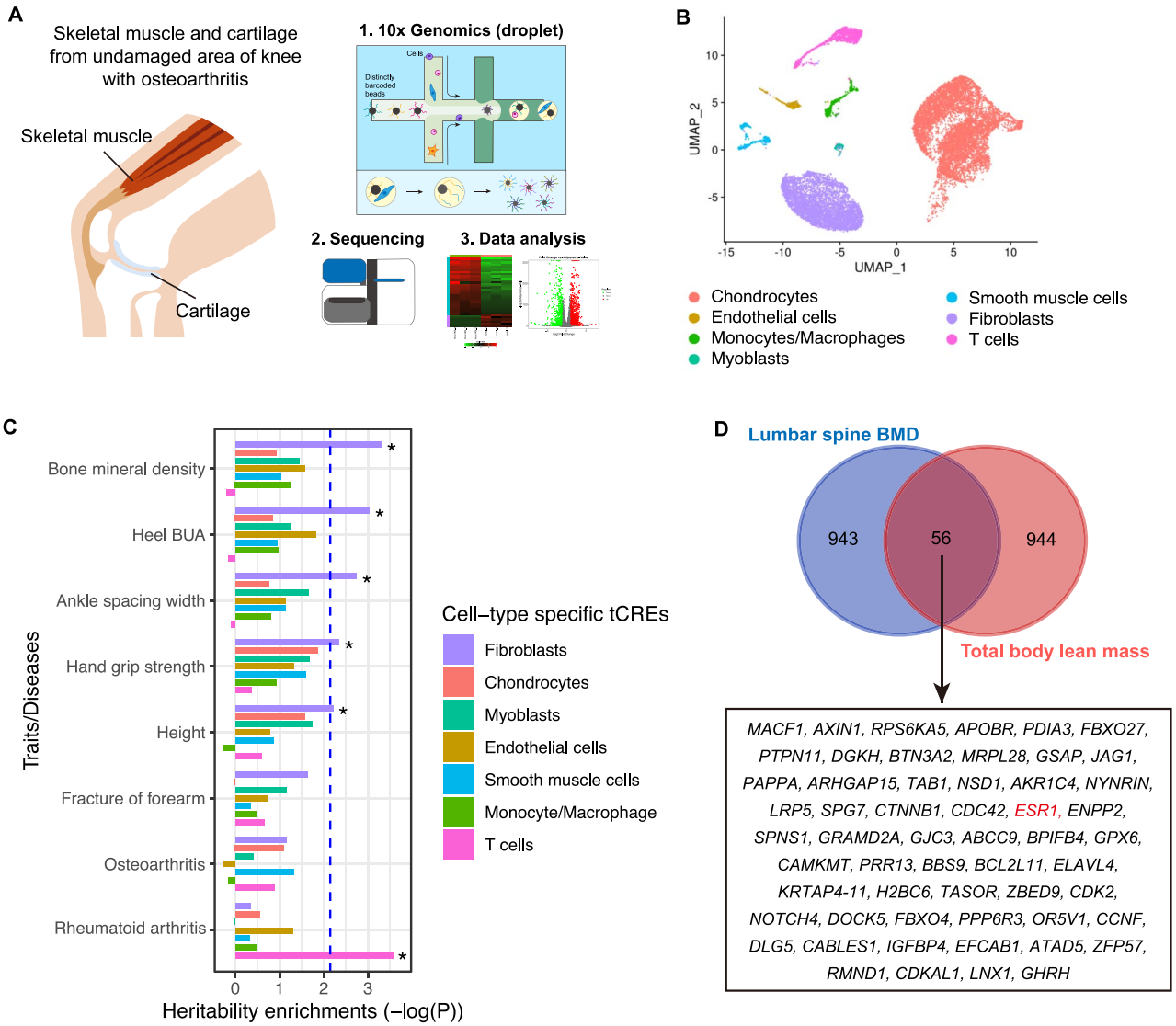

Figure 1. Fibroblasts from skeletal muscle correlated with BMD, and *ESR1* is the common gene regulating both muscle and bone mass. (A) The scRNA-seq process. (B) Single-cell clusters based on cell types. (C) Association of trait heritability to cell types. (D) Common association genes between LS BMD and total body lean mass from Musculoskeletal Knowledge Portal data.

they regulate muscle mass and function. To investigate the function of *Esr1* on PDGFRα+ cells, we generated PDGFRα+ cells-specific *Esr1* KO mice by crossing them with $PDGFR\alpha^{CreERT}$ mice and $Esr1^{fl/fl}$ mice. Tamoxifen (TMX) was injected at 11 wk of age and mice were sacrificed at 23 wk of age (Figure 2A). $Esr1^{fl/fl}$, $PDGFR\alpha^{CreERT}$, and $PDGFR\alpha^{CreERT}$;$Esr1^{fl/+}$ were used as controls, because there was no difference in the bone phenotypes between genotypes (Figure S2). *Esr1* expression levels in PDGFRα+ cells from muscles were significantly lower in $Esr1^{\Delta P\alpha}$ cells compared to controls (Figure 2B). Although there were no differences in body weight, uterus weight, muscle weight, grip strength, or fat weight (Figure 2C-G), distal femoral BMD by DXA was significantly lower in $Esr1^{\Delta P\alpha}$ mice compared to controls (Figure 2H). Then, since a difference in BMD was observed in metaphyseal region of the distal femur, bone structure analysis was performed in this region using μCT. As a result, cortical bone thickness was significantly lower in the $Esr1^{\Delta P\alpha}$ mice compared to controls (Figure 3A and B). In contrast, trabecular bone parameters and bone marrow fat volume were not different between genotypes (Figure 3C-F). Analysis of cortical bone perimeter revealed a significant increase in periosteal and endosteal perimeter in $Esr1^{\Delta P\alpha}$ mice compared to control mice (Figure 4B-E), indicating that the cortical bone of $Esr1^{\Delta P\alpha}$ mice has an expanded marrow cavity. We also analyzed aged mice at 20-24 mo of age (Figure S3A). Consistent with 23-wk-old mice, body weight, muscle weight, grip strength, and fat weight were not different between the control and $Esr1^{\Delta P\alpha}$ mice (Figure S3B-F). However, femoral BMD also was not different between the genotypes (Figure S3G), suggesting that the bone phenotypes regulated by estrogen signaling in PDGFRα+ cells is not apparent after spontaneous estrogen deficiency. Moreover, to investigate sex difference, we analyzed $Esr1^{\Delta P\alpha}$ male mice. As results, there was no difference in body weight, muscle weight, grip strength, fat weight, and BMD between control and cKO (Figure S4A-G). These results suggest that estrogen signaling in PDGFRα+ cells is more important to female's bone than male.

To analyze the dynamics of osteoblasts and osteoclasts, bone histomorphometry was performed on 4 separate areas of

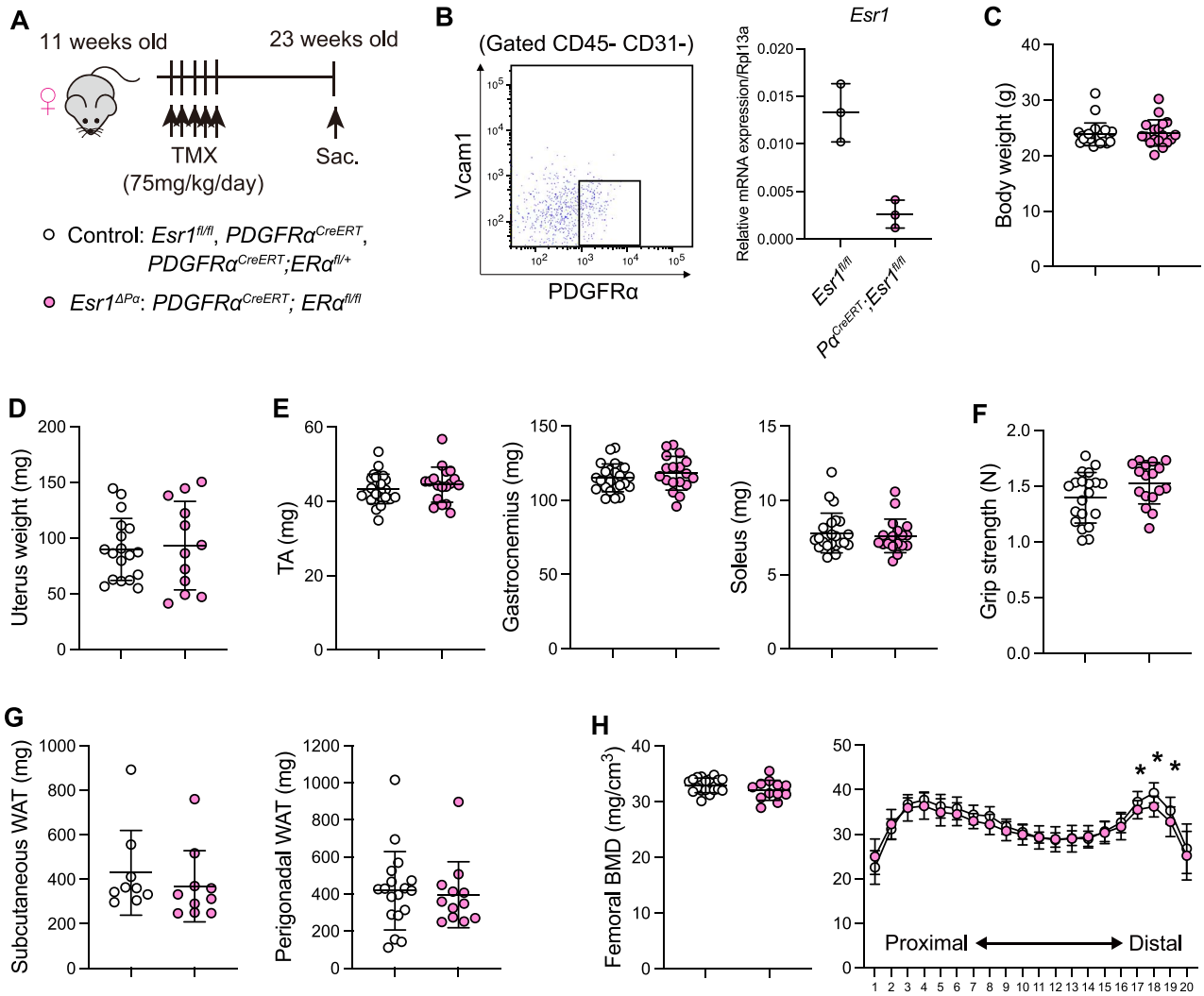

Figure 2. *Esr1*$^{\Delta Pα}$ mice had lower BMD in the distal femur. (A) Experimental protocol. Tamoxifen (TMX) was injected into 11-wk-old female mice, which were sacrificed at 23 wk of age. (B) Sorting gate by FCAS and *Esr1* expression level of PDGFRα+ cells from skeletal muscles in *Esr1*$^{\Delta Pα}$ and control mice. $n = 3$ biological replicates for each strain. (C) Body weight. (D) Uterus weight. (E) Wet weight of tibial anterior (TA), gastrocnemius, and soleus muscles. (F) Grip strength of the forelimb. (G) Wet weight of subcutaneous and perigonadal white adipose tissue (WAT). (H) Total femoral BMD (left) and BMD at each site when the bone is divided into 20 sections (right). The open dots and coloured dots indicate control and *Esr1*$^{\Delta Pα}$ respectively. Data are presented as means ± SD. *, $p < .05$ by nonparametric Mann–Whitney U test. $n = 18$-24 biological replicates for each strain.

cortical bone in the distal femur (endosteum and periosteum, posteriorly and anteriorly) in control and *Esr1*$^{\Delta Pα}$ mice at 23 wk of age (Figure 5A-J). Bone formation rate/bone surface (BFR/BS) in the posterior endosteum was significantly greater in *Esr1*$^{\Delta Pα}$ mice compared to controls (Figure 5A and B). Also, osteoclast surface/bone surface (Oc.S/BS) and osteoclast number/bone perimeter (N.Oc/B.Pm) in posterior periosteum by TRAP staining were significantly increased in *Esr1*$^{\Delta Pα}$ mice compared to controls (Figure 5F and H). On the other hand, osteoblast surface and number were no changed between groups (Figure 5F-J). Consistent with TRAP staining, toluidine blue staining also showed an increase in osteoclast-like cells in the periosteum of *Esr1*$^{\Delta Pα}$ mice (Figure 5F). These results suggest that *Esr1*$^{\Delta Pα}$ mice had low bone mass because of a high turnover bone phenotype.

Esr1$^{\Delta Pα}$ mice showed higher *Igfbp5* levels, both in gene expression in PDGFRα+ cells and serum concentration

To examine the effect of *Esr1* ablation on PDGFRα+ cells in bone, we performed bulk RNA-seq in PDGFRα+ cells obtained from bone of both control and *Esr1*$^{\Delta Pα}$ mice (Figure S5A). PDGFRα+ cells were isolated from distal femur and proximal tibia and, including growth plate, because of the difference in BMD between controls and *Esr1*$^{\Delta Pα}$ around metaphyseal region of the distal femur. The number of PDGFRα+ cells was not different between control and *Esr1*$^{\Delta Pα}$ (Figure S5B). The principal component analysis (PCA) plot showed no separation between the control and *Esr1*$^{\Delta Pα}$ samples (Figure S5C). Also, we could not identify differentially expressed genes between *Esr1*$^{\Delta Pα}$ and control mice (Figure S5D).

To investigate of the effect of *Esr1* ablation on PDGFRα+ cells in skeletal muscles, we performed Bulk RNA-seq in PDGFRα+ cells from skeletal muscles of both control and *Esr1*$^{\Delta Pα}$ mice (Figure 6A). Using a previously established gating strategy for PDGFRα+ cells from muscles (CD45− CD31− Vcam1− PDGFRα+)[37] (Figure 6B), we isolated PDGFRα+ cells from lower limb muscles for RNA-seq. The number of PDGFRα+ cells were not different between control and *Esr1*$^{\Delta Pα}$ (Figure 6B). The PCA plot revealed separation between the control and *Esr1*$^{\Delta Pα}$

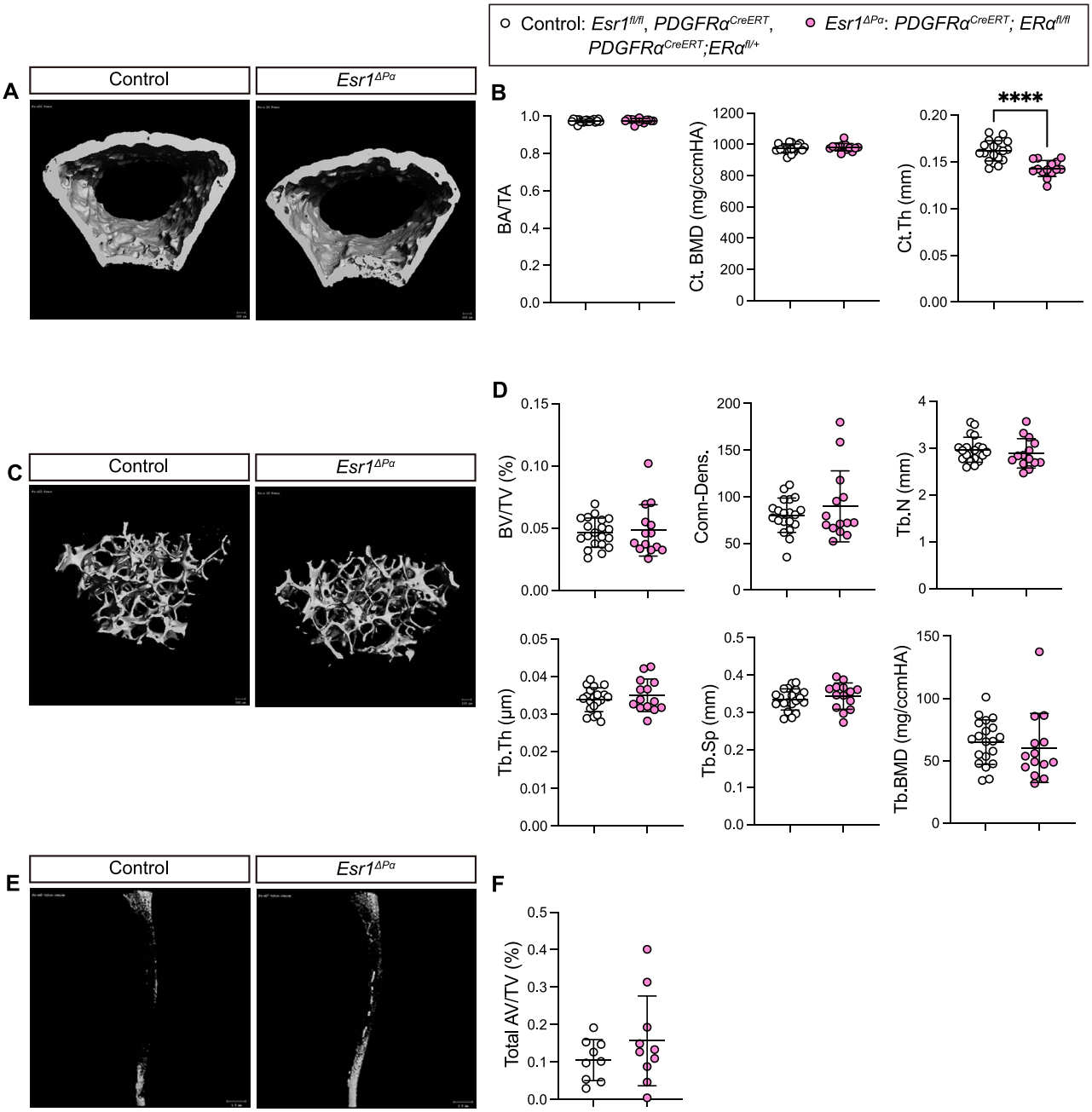

Figure 3. *Esr1*$^{\Delta Pα}$ mice exhibited low cortical bone thickness at the distal femur. (A) Representative image of cortical bone in distal femur of *Esr1*$^{\Delta Pα}$ and control mice. (B) Bone area/tissue area (BA/TA), cortical (Ct) BMD, and cortical thickness (Ct.Th). (C) Representative image of trabecular bone in the distal femur of *Esr1*$^{\Delta Pα}$ and control mice. (D) Bone volume/tissue volume (BV/TV), trabecular thickness (Tb.Th), and trabecular (Tb) BMD, trabecular space (Tb.Sp), trabecular number (Tb.N), and connective density (Conn-Dens). $n = 13$-20 biological replicates for each strain. (E) Representative image of bone marrow fat in the femur of *Esr1*$^{\Delta Pα}$ and control mice. (F) Total adipocyte volume/total volume (AV/TV). $n = 9$-10 biological replicates for each strain. Data are presented as means ± SD. ****, $p < .0001$ by nonparametric Mann–Whitney U test.

samples (Figure 6C). We identified 10 upregulated and 11 downregulated genes in PDGFRα+ cells from the *Esr1*$^{\Delta Pα}$ mice (Figure 6D). The heatmap indicated upregulated genes, including *Col1a2*, *Igfbp5*, and *Adamts12*, related to the secreted factors by *Esr1* ablation (Figure 6E). Further, gene enrichment analysis of the upregulated genes ($p < .01$) revealed that those genes were enriched for "regulation of osteoblast differentiation" (Figure 6F). Among the genes categorized in "regulation of osteoblast differentiation," *Igfbp5* was identified as the most significantly upregulated gene (Figure 6G). In addition, serum IGFBP5 concentration was significantly higher in *Esr1*$^{\Delta Pα}$ compared to control mice (Figure 6H).

IGFBP5 suppressed osteoblast differentiation and accelerated osteoclast differentiation

According to enrichment analysis, *Igfbp5* was included in the gene ontology term indicating the regulation of osteoblast differentiation. Mukherjee and Rotwein[29] reported that IGFBP5 inhibits osteogenesis by blocking insulin-like growth factor (IGF) actions. To confirm the effect of

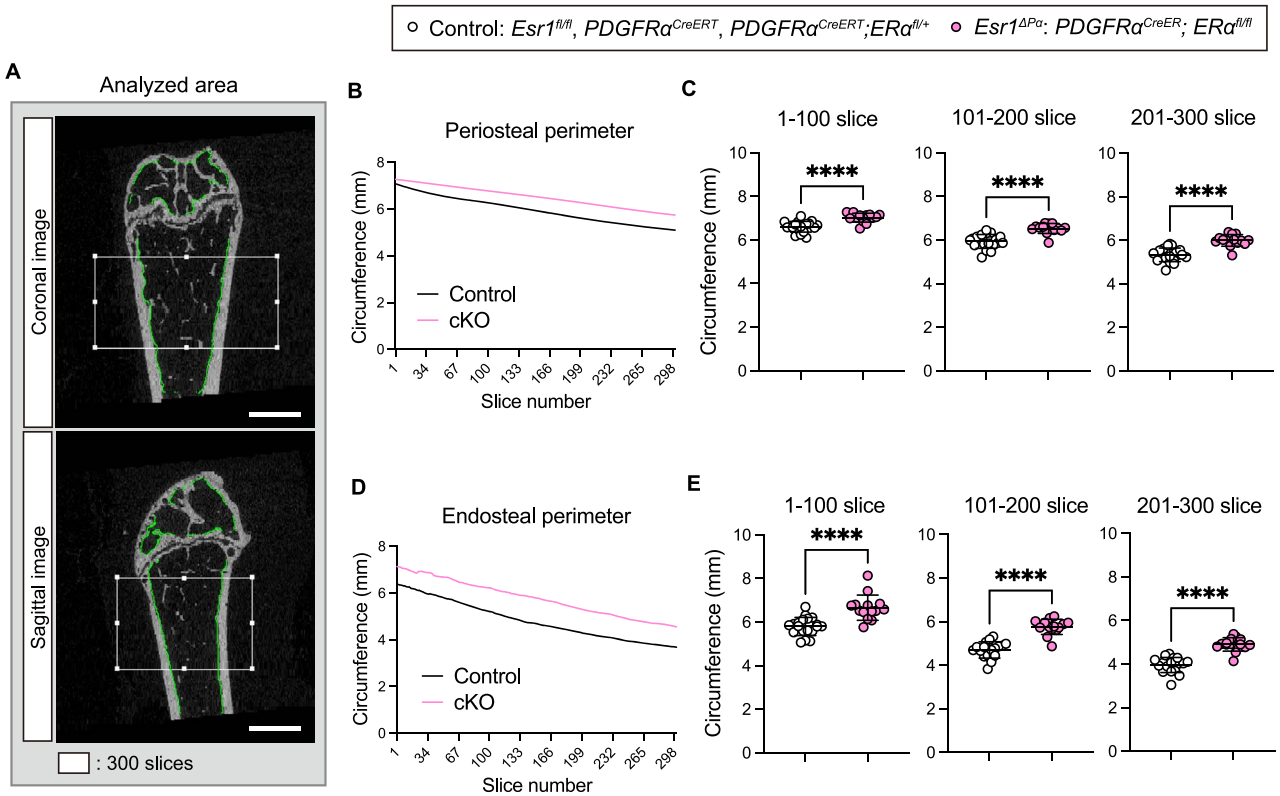

Figure 4. *Esr1*$^{\Delta Pα}$ mice exhibited increasing in periosteal and endosteal perimeter. (A) Image of the analyzed area. The square indicates the analyzed area (300 slices). The line of inside bone indicates the boundary between cortical bone and trabecular bone. Scale bars indicate 1 mm. (B) Plot of periosteal perimeter of 300 slices and (C) average values for every 100 slices. (D) Plot of endosteal perimeter of 300 slices and (E) average values for every 100 slices. Data are presented as means ± SD. ****, $p < .0001$ by nonparametric Mann–Whitney U test.

IGFBP5 on osteoblast differentiation, we cultured MC3T3-E1 cells, an osteoblast-like cell line, with or without IGFBP5 recombinant protein and assessed differentiation capacity by alkaline phosphatase (ALP) staining. The ALP staining area was significantly lower in MC3T3-E1 cells treated with IGFBP5 compared to control cells (Figure 7A and B). IGFBP5-treated cells had significantly lower expression in the early-stage marker genes of osteoblasts, such as *Osx* and *Runx2*, compared to control cells (Figure 7C). Furthermore, since it has been reported that IGFBP5 promotes osteoclast formation and osteoclastic resorbing activity,[38] we also cultured RAW264 cells, a macrophage-like cell line, with or without IGFBP5 recombinant protein. This demonstrated that RANKL-induced osteoclast differentiation was facilitated by IGFBP5 treatment (Figure 7D and E). These data suggest that *Igfbp5*/IGFBP5 signaling attenuates bone metabolism.

Next, to investigate the effect of secreted factors from *Esr1* deleted PDGFRα+ cells for osteoblast differentiation, we collected conditioned medium from cultured PDGFRα+ cells obtained from both control and *Esr1*$^{\Delta Pα}$ mice, and cultured primary calvarial osteoblasts with the conditioned medium (Figure S6A). Alkaline phosphatase staining revealed that there was no difference between groups (Figure S6B and C), suggesting that secreted factors from *Esr1* deleted PDGFRα+ cells not affected to osteoblast differentiation in vitro under this condition.

Discussion

In this study, we investigated the action of *Esr1* in PDGFRα+ cells to maintain bone mass and muscle function using *Esr1*$^{\Delta Pα}$ mice based on scRNA-seq data in human samples. We found that deletion of estrogen signaling in PDGFRα+ cells promotes *Igfbp5* secretion from PDGFRα+ cells and induces cortical bone loss. These results suggest that *Esr1* signaling in PDGFRα+ cells plays a significant role to maintain bone mass.

The bone mass-maintaining effect of estrogen is the sum of direct and indirect effects. Direct effects of estrogen on bone have been revealed by various bone cell-specific *Esr1* KO mice. Osteoclast-specific *Esr1* KO mice have low trabecular bone mass with high bone turnover accelerated by apoptosis through FasL expression.[3] Furthermore, osteoblast/osteocyte-specific *Esr1* KO mice have been studied by osteoblast/osteocyte differentiation stage. Osteoblast progenitor-specific *Esr1* KO mice have low cortical bone mass through reduction of Wnt/β-catenin signaling in periosteal osteoblasts.[4] Also, mature osteoblast-specific *Esr1* KO mice have decreased trabecular and cortical bone mass with low bone turnover.[39] In addition, osteocyte-specific *Esr1* KO mice have low trabecular bone mass with decreased bone formation; Wnt signaling was implicated in this mechanism.[5,6] On the other hand, estrogen regulates bone homeostasis via various indirect effects. As estrogen negatively regulates inflammatory cytokines, such as TNF-α, IL-1, and IL-7, estrogen deficiency can induce secretion of inflammatory cytokines from immune cells, and accelerate osteoclastogenesis, subsequently decreasing bone mass.[7] Also, estrogen deficiency-induced secretion of FSH from the pituitary gland stimulates osteoclastogenesis and accelerates bone resorption.[8] Furthermore, estrogen deficiency causes a gut microbiome-dependent expansion of Th17 cells and TNF-α-producing T cells in bone marrow. However, blockade of

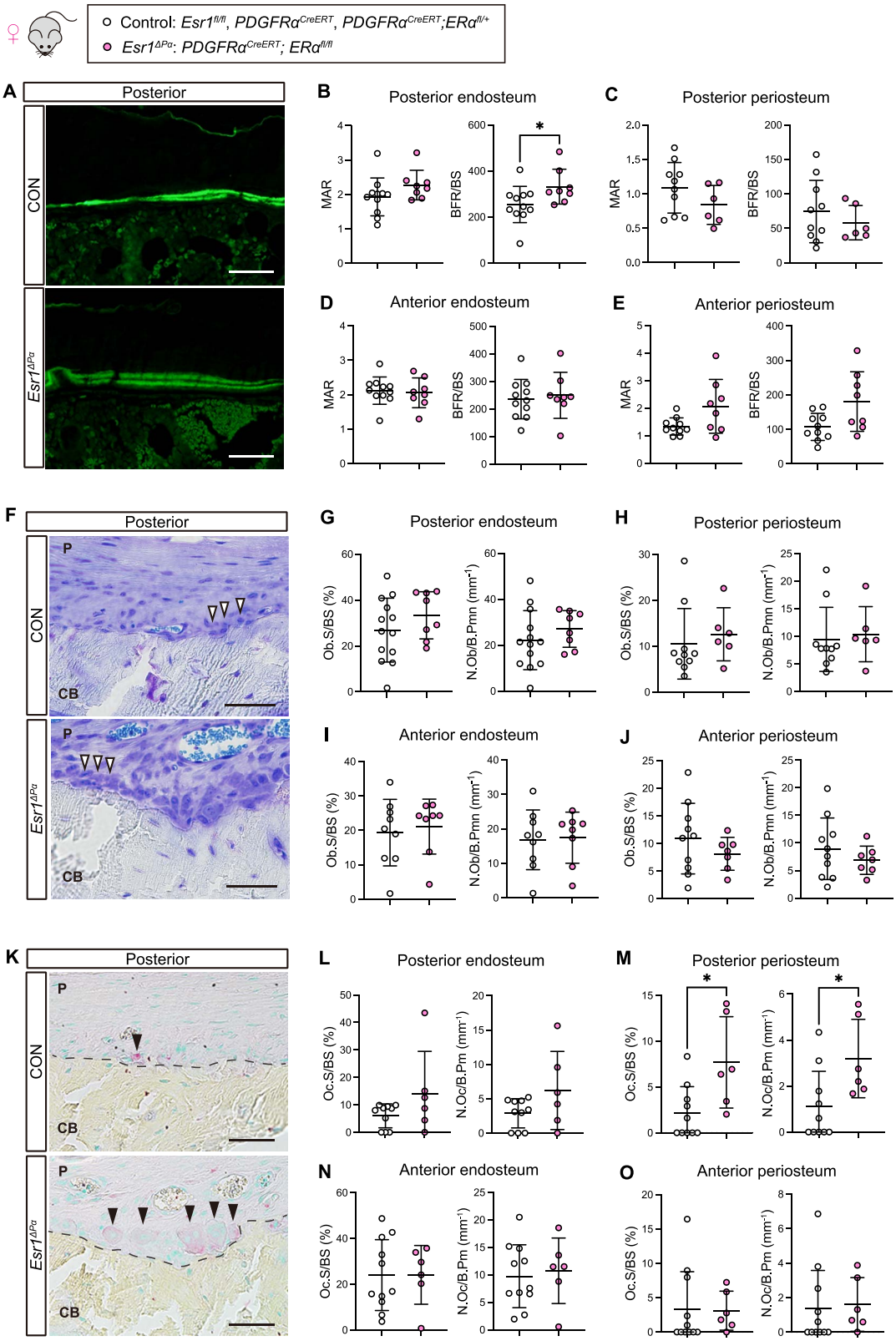

Figure 5. *Esr1*$^{\Delta Pα}$ mice had low bone mass and high bone turnover. (A) Representative image of calcein labeling in the distal femoral cortical bone of *Esr1*$^{\Delta Pα}$ and control mice. Scale bars indicate 50 μm. Mineral apposition rate (MAR) and bone formation rate/bone surface (BFR/BS) in (B) posterior endosteum, (C) posterior periosteum, (D) anterior endosteum, and (E) anterior periosteum. $n = 8$-11 biological replicates for each strain. (F) Representative image of toluidine blue staining in the distal femoral cortical bone of *Esr1*$^{\Delta Pα}$ and control mice. P indicates periosteum. CB indicates cortical bone. Scale bars indicate 50 μm. Osteoblast surface/bone surface (Ob.S/BS) and osteoblast number/bone perimeter (N.Oc/B.Pm) in (G) posterior endosteum, (H) posterior periosteum, (I) anterior endosteum, and (J) anterior periosteum. $n = 6$-13 biological replicates for each strain. (K) Representative image of TRAP staining in the distal femoral cortical bone of *Esr1*$^{\Delta Pα}$ and control mice. Scale bars indicate 50 μm. Osteoclast surface/bone surface (Oc.S/BS) and osteoclast number/bone perimeter (N.Oc/B.Pm) in (L) posterior endosteum, (M) posterior periosteum, (N) anterior endosteum, and (O) anterior periosteum. The open dots and coloured dots indicate control and *Esr1*$^{\Delta Pα}$ respectively. $n = 7$-12 biological replicates for each strain. Data are presented as means ± SD. *, $p < .05$ by nonparametric Mann–Whitney U test.

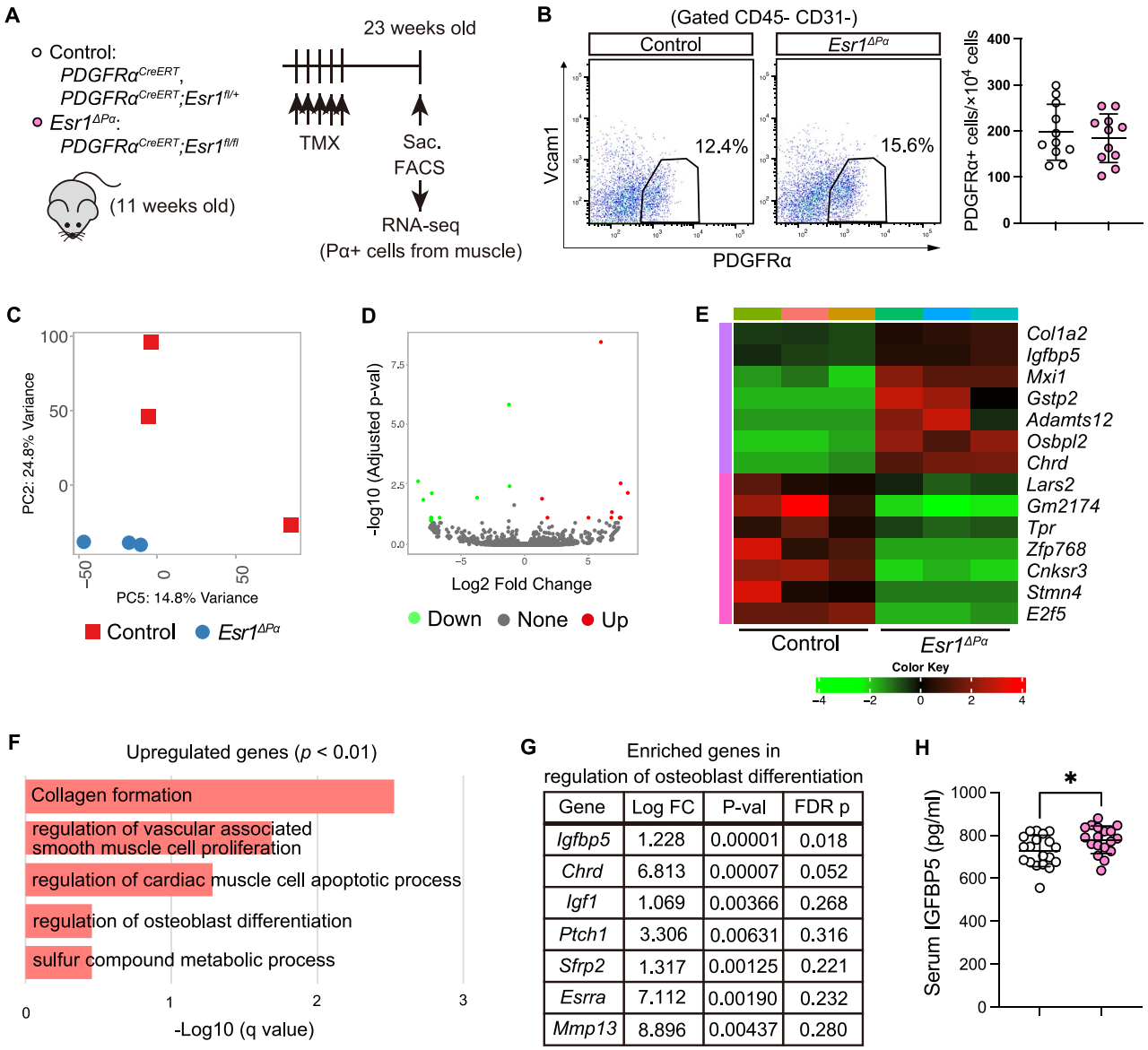

Gene	Log FC	P-val	FDR p
Igfbp5	1.228	0.00001	0.018
Chrd	6.813	0.00007	0.052
Igf1	1.069	0.00366	0.268
Ptch1	3.306	0.00631	0.316
Sfrp2	1.317	0.00125	0.221
Esrra	7.112	0.00190	0.232
Mmp13	8.896	0.00437	0.280

Figure 6. *Igfbp5* expression was higher in PDGFRα+ cells derived from muscle in *Esr1*$^{\Delta P\alpha}$ mice. (A) Female mice injected with TMX at 12 wk of age were sacrificed at 23 wk and PDGFRα+ cells were isolated from lower limb muscles for RNA-seq. $n = 3$ biological replicates for each strain. (B) Sorting gate of PDGFRα+ cells by FACS (left) and number of PDGFRα+ cells in *Esr1*$^{\Delta P\alpha}$ and control mice (right). (C) Principal component analysis (PCA) plot. (D) Volcano plot. (E) Heat map of top 15 differentially expressed genes. (F) Enrichment analysis of upregulated genes. The bars represent -log10 q-values of these genes. (G) Genes enriched for regulation of osteoblast differentiation. (H) Serum IGFBP5 concentration. Data are presented as means ± SD. *, $p < .05$ by nonparametric Mann–Whitney U test.

Th17 cell and TNF+ T cell egress from the gut or their influx into the bone marrow prevented OVX-induced bone loss.[40] Therefore, estrogen is involved in bone health through regulation of various physiological functions. Among these, our findings show a novel action of estrogen in PDGFRα+ cells.

Consistent with the high-turnover osteoporosis observed in postmenopausal women and in ovariectomized mice,[41] *Esr1*$^{\Delta P\alpha}$ mice developed a high-turnover bone phenotype. Of note, bone loss in *Esr1*$^{\Delta P\alpha}$ mice was specifically detected in the cortical bone of the distal femur. This regional specificity may be attributable to the proximity of the distal femur to the muscle–tendon junction, rendering the site more sensitive to mechanical stress or secreted molecules from soft tissues. In addition, bone histomorphometry revealed increased osteoclast numbers and bone formation rates in the posterior cortical region, suggesting that mechanical stress may contribute to this phenotype. Consistent with previous study,[42] osteoclasts and osteoblasts were located at the opposite sides of a cortical bone.

Esr1$^{\Delta P\alpha}$ mice exhibited a significant increase in periosteal and endosteal perimeter, indicating that marrow cavity expanded. Previous study reported that estrogen acting via *Esr1* suppresses periosteal apposition and endocortical resorption. Therefore, postmenopausal women[43] and estrogen deficient rodents[44] result in enlargement of both periosteal and endocortical diameters. Thus, our data suggest that the effects of estrogen on endocortical and periosteal surfaces are mediated by *Esr1* in PDGFRα+ cells.

PDGFRα+ cells are localized in various tissues,[32,45] and also exist in bone, such as skeletal stem cells and osteoblast lineage cells.[33] PDGFRα+ cells in bone could act directly

Figure 7

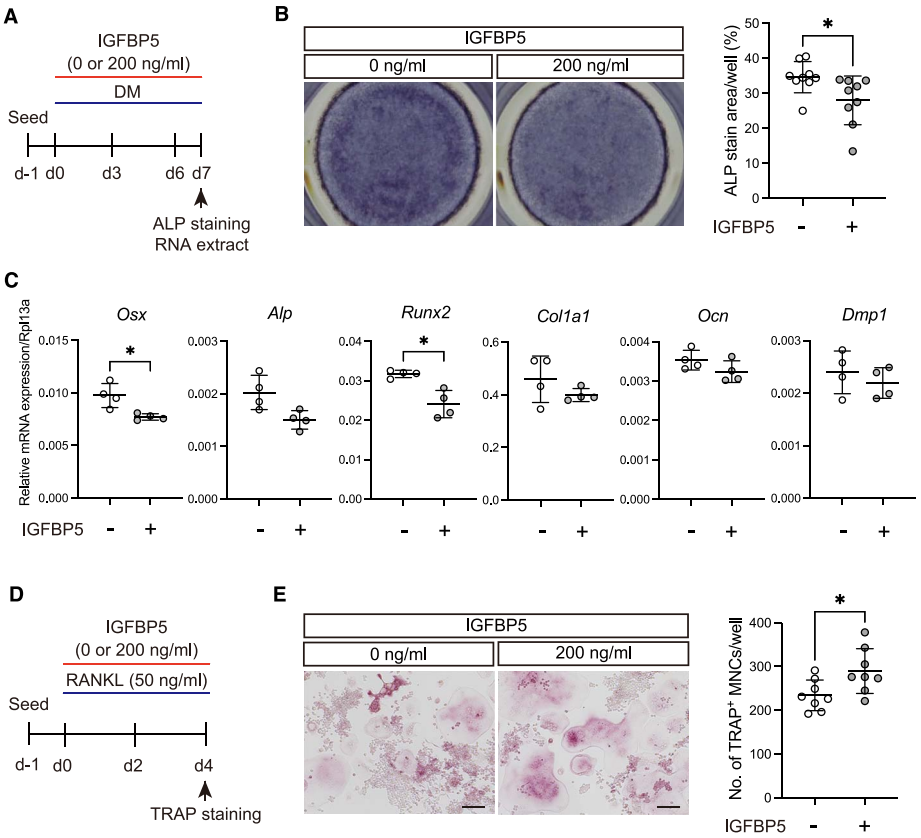

Figure 7. Recombinant IGFBP5 protein suppressed osteoblast differentiation and facilitated osteoclastogenesis in vitro. (A) Osteoblast differentiation experimental protocol using MC3T3-E1 cells. DM: differentiation medium (B) representative image of ALP staining by 0 or 200 ng/mL IGFBP5 administration (left) and quantitative data of ALP staining area. $n = 9$ biological replicates from 3 technical replicates for each condition. (C) Gene expression level in 7 d cultured MC3T3-E1 cells with or without IGFBP5 by RT-qPCR. (D) Experimental protocol for the differentiation of RAW264 cells into osteoclasts by RANKL. (E) Representative image of TRAP staining of multinucleated osteoclasts (MNCs) and quantitative data of number of TRAP+ MNCs/well. $n = 8$ biological replicates from 2 technical replicates for each strain. Scale bars indicate 100 μm. Data are presented as means ± SD. *, $p < .05$ by nonparametric Mann–Whitney U test.

on bone via estrogen signaling to regulate bone mass, while no differentially expressed genes were found from RNA-seq data from bone between *Esr1*$^{\Delta Pα}$ and control mice. PDGFRα+ cells were collected from the distal femur and proximal tibia, including the growth plate, for RNA-seq analysis. Considering that the phenotype observed in *Esr1*$^{\Delta Pα}$ mice is relatively mild, highly localized, and restricted to cortical bone, the effects of *Esr1* deficiency in specific cell populations might be masked by the heterogeneity of the isolated PDGFRα+ cells. Furthermore, previous reports showed that osteoblast-specific *Esr1* KO mice exhibited different type of bone loss phenotype with differentiation stages. When compared with these previous reports, the bone phenotype of *Esr1*$^{\Delta Pα}$ exhibited low cortical bone thickness as similar to osteoblast progenitors-specific *Esr1* KO mice[4] and also exhibited periosteal and endosteal expansion as similar to osteocyte-specific *Esr1* KO mice.[6] Therefore, it is possible that PDGFRα+ cells contribute to abnormal bone phenotype of *Esr1*$^{\Delta Pα}$ in a different way. In addition, it is also possible that *Igfbp5* expression is increased from PDGFRα+ cells in other tissues, but this does not necessarily mean that PDGFRα+ cells in muscle and other tissues show similar gene expression, because it has been reported that PDGFRα+ cells have tissue-specific functions, such as various differentiation potential and gene expression signatures.[45] Therefore, further research is needed to clarify this point.

Esr1 deletion in PDGFRα+ cells did not affect skeletal muscle mass and grip strength. Uezumi et al.[37] reported that depletion of PDGFRα+ mesenchymal progenitors using *Pdgfrα-CreERT*+/R26-DTA mice leads to muscle weakness, myofiber atrophy, alterations of fiber types and denervation at neuromuscular junctions. In addition, with respect to skeletal muscle regulation via PDGFRα+ cells by sex hormones, androgen receptor deletion in PDGFRα+ cells have been reported to induce lower limb muscle mass via lower *Igf1* expression in mature male mice.[46] These previous studies suggest that PDGFRα+ mesenchymal progenitors have an important role to maintain muscle mass and function, and that androgen is a key regulator to control PDGFRα+ mesenchymal progenitors in male mice. However, our findings suggest that *Esr1* action has a limited role to maintain skeletal muscle homeostasis via PDGFRα+ cells in female mice.

Our results showed that male *Esr1*$^{\Delta Pα}$ mice did not show bone loss phenotype. Previous studies on several *Esr1* or *Esr2* KO mice[4,6,12] have also shown that the phenotype is milder in males than in females, and thus the effects of estrogen on PDGFRα+ cells are also milder in males than in females.

There are some limitations to this study. First, it is still unclear how *Esr1* suppresses *Igfbp5* expression in PDGFRα+ cells. As there are few reports on the transcriptional repression by ERα, it may regulate *Igfbp5* via some unknown factors. Soriano-Arroquia et al.[34] reported that miR-143 regulates *Igfbp5* mRNA stability. In addition, it has been recently reported that the mice lacking *Esr1* in arcuate nucleus (ARC) highly expressed *Ccn3* gene in ARC, then exhibited high bone mass.[47] Therefore, the mechanism underlying transcriptional regulation of *Igfbp5* by ERα requires further study. Second, $PDGFR\alpha^{CreERT}$ mice did not specifically express CreERT in bone or skeletal muscle PDGFRα+ cells; therefore, the mice used in this study were mice lacking *Esr1* in PDGFRα+ cells throughout the body.

In conclusion, the results of this study suggest that estrogen signaling in PDGFRα+ cells suppresses *Igfbp5* expression, then maintains bone mass, indicating that *Esr1* signaling in PDGFRα+ cells plays a significant role in bone metabolism.

Acknowledgments

We thank the staff of the Division of Analytical Bio-Medicine and the Division of Laboratory Animal Research, the Advanced Research Support Center (ADRES), the members of the Division of Integrative Pathophysiology, Proteo-Science Center (PROS), and Ehime University for their technical assistance and helpful support. This publication is a part of the Single Cell Medical Network in Japan.

Author contributions

Aoi Ikedo (Conceptualization, Methodology, Formal analysis, Investigation, Data curation, Writing—original draft, Visualization), Reina Aoki (Conceptualization, Methodology, Formal analysis, Investigation, Data curation, Visualization), Hiroshi Sakai (Methodology, Investigation, Writing—review & editing), Noritaka Saeki (Methodology, Writing—review & editing), Yuta Yanagihara (Formal analysis, Data curation), Jonathan Moody (Conceptualization, Methodology, Formal analysis, Investigation, Data curation, Writing—review & editing, Visualization), Miki Kojima (Single-cell RNAseq experiment), Tsukasa Kouno (Single-cell RNAseq experiment), Yoshinari Ando (Single-cell RNAseq experiment, Writing—review & editing), Kazunori Hino (Methodology, Writing—review & editing), Tomofumi Kinoshia (Methodology, Writing—review & editing), Piero Carninci (Single-cell RNAseq experiment, Writing—review & editing), Jay W. Shin (Conceptualization, Methodology, Formal analysis, Investigation, Data curation, Writing—review & editing, Visualization), Chung-Chau Hon (Conceptualization, Methodology, Formal analysis, Investigation, Data curation, Writing—review & editing, Visualization), Akiyoshi Uezumi (Methodology, Writing—review & editing), Yoshiaki Kamei (Supervision, Writing—review & editing), and Yuuki Imai (Conceptualization, Methodology, Resources, Funding acquisition, Project administration, Supervision, Writing—review & editing)

Supplementary material

Supplementary material is available at *JBMR Plus* online.

Funding

This work was supported in part by JSPS KAKENHI JP22H03203 and JP23K24462 to Y.I. and by a research grant to the RIKEN Center for Integrative Medical Sciences (IMS) from the Ministry of Education, Culture, Sports, Science and Technology (MEXT).

Conflicts of interest

The authors declare no conflict of interests.

Data availability

RNA-seq data have been deposited in the Gene Expression Omnibus as accession number GSE279051. Sequencing data of the single-cell RNA-seq are available in NBDC at https://humandbs.dbcls.jp/en with accession [in process].

Ethics approval statement

All animal experiments were approved by the Animal Experiment Committee of Ehime University (Approval No. 37A1-1·16) and were conducted in full compliance with the Guidelines for Animal Experiments at Ehime University.

Patient consent statement

All human samples examined in this study were either exempted materials or obtained with informed consent, and were covered under the following research protocols at Ehime University Hospital IRB (1812005). Written informed consent was obtained from all participants for sample collection, data acquisition, usage, and publication.

References

1. Yoshimura N, Muraki S, Oka H, et al. Do sarcopenia and/or osteoporosis increase the risk of frailty? A 4-year observation of the second and third ROAD study surveys. *Osteoporos Int*. 2018;29(10):2181-2190. https://doi.org/10.1007/s00198-018-4596-4
2. Kirk B, Zanker J, Duque G. Osteosarcopenia: epidemiology, diagnosis, and treatment-facts and numbers. *J Cachexia Sarcopenia Muscle*. 2020;11(3):609-618. https://doi.org/10.1002/jcsm.12567
3. Nakamura T, Imai Y, Matsumoto T, et al. Estrogen prevents bone loss via estrogen receptor alpha and induction of Fas ligand in osteoclasts. *Cell*. 2007;130(5):811-823. https://doi.org/10.1016/j.cell.2007.07.025
4. Almeida M, Iyer S, Martin-Millan M, et al. Estrogen receptor-α signaling in osteoblast progenitors stimulates cortical bone accrual. *J Clin Invest*. 2013;123(1):394-404. https://doi.org/10.1172/jci65910
5. Kondoh S, Inoue K, Igarashi K, et al. Estrogen receptor α in osteocytes regulates trabecular bone formation in female mice. *Bone*. 2014;60:68-77. https://doi.org/10.1016/j.bone.2013.12.005
6. Doolittle ML, Saul D, Kaur J, et al. Skeletal effects of inducible ERalpha deletion in osteocytes in adult mice. *J Bone Miner Res*. 2022;37(9):1750-1760. https://doi.org/10.1002/jbmr.4644
7. Pacifici R. Estrogen deficiency, T cells and bone loss. *Cell Immunol*. 2008;252(1-2):68-80. https://doi.org/10.1016/j.cellimm.2007.06.008
8. Sun L, Peng Y, Sharrow AC, et al. FSH directly regulates bone mass. *Cell*. 2006;125(2):247-260. https://doi.org/10.1016/j.cell.2006.01.051
9. Greendale GA, Sternfeld B, Huang M, et al. Changes in body composition and weight during the menopause transition. *JCI. Insight*. 2019;4(5):e124865. https://doi.org/10.1172/jci.insight.124865
10. Sipilä S, Törmäkangas T, Sillanpää E, et al. Muscle and bone mass in middle-aged women: role of menopausal status and physical activity. *J Cachexia Sarcopenia Muscle*. 2020;11(3):698-709. https://doi.org/10.1002/jcsm.12547
11. Kitajima Y, Ono Y. Estrogens maintain skeletal muscle and satellite cell functions. *J Endocrinol*. 2016;229(3):267-275. https://doi.org/10.1530/joe-15-0476
12. Seko D, Fujita R, Kitajima Y, Nakamura K, Imai Y, Ono Y. Estrogen receptor β controls muscle growth and regeneration in young female mice. *Stem Cell Rep*. 2020;15(3):577-586. https://doi.org/10.1016/j.stemcr.2020.07.017
13. Moody J, Kouno T, Kojima M, et al. A single-cell atlas of transcribed cis-regulatory elements in the human genome. *bioRxiv*. 2023. https://doi.org/10.1101/2023.11.13.566791

14. Liu L, Cheung TH, Charville GW, Rando TA. Isolation of skeletal muscle stem cells by fluorescence-activated cell sorting. *Nat Protoc*. 2015;10(10):1612-1624. https://doi.org/10.1038/nprot.2015.110
15. Fleming SJ, Chaffin MD, Arduini A, et al. Unsupervised removal of systematic background noise from droplet-based single-cell experiments using CellBender. *Nat Methods*. 2023;20(9):1323-1335. https://doi.org/10.1038/s41592-023-01943-7
16. Wolock SL, Lopez R, Klein AM. Scrublet: computational identification of cell doublets in single-cell transcriptomic data. *Cell Syst*. 2019;8(4):281-291.e9. https://doi.org/10.1016/j.cels.2018.11.005
17. Polański K, Young MD, Miao Z, Meyer KB, Teichmann SA, Park JE. BBKNN: fast batch alignment of single cell transcriptomes. *Bioinformatics*. 2020;36(3):964-965. https://doi.org/10.1093/bioinformatics/btz625
18. Bernstein MN, Ma Z, Gleicher M, Dewey CN. CellO: comprehensive and hierarchical cell type classification of human cells with the Cell Ontology. *iScience*. 2021;24(1):101913. https://doi.org/10.1016/j.isci.2020.101913
19. Stuart T, Butler A, Hoffman P, et al. Comprehensive integration of single-cell data. *Cell*. 2019;177(7):1888-1902.e21. https://doi.org/10.1016/j.cell.2019.05.031
20. Moody J, Kouno T, Chang JC, et al. SCAFE: a software suite for analysis of transcribed cis-regulatory elements in single cells. *Bioinformatics*. 2022;38(22):5126-5128. https://doi.org/10.1093/bioinformatics/btac644
21. Finucane HK, Reshef YA, Anttila V, et al. Heritability enrichment of specifically expressed genes identifies disease-relevant tissues and cell types. *Nat Genet*. 2018;50(4):621-629. https://doi.org/10.1038/s41588-018-0081-4
22. Heinz S, Benner C, Spann N, et al. Simple combinations of lineage-determining transcription factors prime cis-regulatory elements required for macrophage and B cell identities. *Mol Cell*. 2010;38(4):576-589. https://doi.org/10.1016/j.molcel.2010.05.004
23. Kang SH, Fukaya M, Yang JK, Rothstein JD, Bergles DE. NG2+ CNS glial progenitors remain committed to the oligodendrocyte lineage in postnatal life and following neurodegeneration. *Neuron*. 2010;68(4):668-681. https://doi.org/10.1016/j.neuron.2010.09.009
24. Dupont S, Krust A, Gansmuller A, Dierich A, Chambon P, Mark M. Effect of single and compound knockouts of estrogen receptors alpha (ERalpha) and beta (ERbeta) on mouse reproductive phenotypes. *Development*. 2000;127(19):4277-4291.
25. Scheller EL, Troiano N, Vanhoutan JN, et al. Use of osmium tetroxide staining with microcomputerized tomography to visualize and quantify bone marrow adipose tissue in vivo. *Methods Enzymol*. 2014;537:123-139. https://doi.org/10.1016/B978-0-12-411619-1.00007-0
26. Zhou Y, Zhou B, Pache L, et al. Metascape provides a biologist-oriented resource for the analysis of systems-level datasets. *Nat Commun*. 2019;10(1):1523. https://doi.org/10.1038/s41467-019-09234-6
27. Maurano MT, Humbert R, Rynes E, et al. Systematic localization of common disease-associated variation in regulatory DNA. *Science*. 2012;337(6099):1190-1195. https://doi.org/10.1126/science.1222794
28. Cho EJ, Takagi T, Moore CR, Buratowski S. mRNA capping enzyme is recruited to the transcription complex by phosphorylation of the RNA polymerase II carboxy-terminal domain. *Genes Dev*. 1997;11(24):3319-3326. https://doi.org/10.1101/gad.11.24.3319
29. Mukherjee A, Rotwein P. Insulin-like growth factorbinding protein-5 inhibits osteoblast differentiation and skeletal growth by blocking insulin-like growth factor actions. *Mol Endocrinol* 2008;22:1238–1250. https://doi.org/10.1210/me.2008-0001
30. Bycroft C, Freeman C, Petkova D, et al. The UK Biobank resource with deep phenotyping and genomic data. *Nature*. 2018;562(7726):203-209. https://doi.org/10.1038/s41586-018-0579-z
31. Kushner PJ, Agard DA, Greene GL, et al. Estrogen receptor pathways to AP-1. *J Steroid Biochem Mol Biol*. 2000;74(5):311-317. https://doi.org/10.1016/s0960-0760(00)00108-4
32. Buechler MB, Pradhan RN, Krishnamurty AT, et al. Cross-tissue organization of the fibroblast lineage. *Nature*. 2021;593(7860):575-579. https://doi.org/10.1038/s41586-021-03549-5
33. Morikawa S, Mabuchi Y, Kubota Y, et al. Prospective identification, isolation, and systemic transplantation of multipotent mesenchymal stem cells in murine bone marrow. *J Exp Med*. 2009;206(11):2483-2496. https://doi.org/10.1084/jem.20091046
34. Soriano-Arroquia A, McCormick R, Molloy AP, McArdle A, Goljanek-Whysall K. Age-related changes in miR-143-3p:Igfbp5 interactions affect muscle regeneration. *Aging Cell* 2016;15:361–369. https://doi.org/10.1111/acel.12442
35. Sivaraj KK, Majev PG, Jeong HW, et al. Mesenchymal stromal cell-derived septoclasts resorb cartilage during developmental ossification and fracture healing. *Nat Commun*. 2022;13(1):571. https://doi.org/10.1038/s41467-022-28142-w
36. Uezumi A, Fukada S, Yamamoto N, Takeda S, Tsuchida K. Mesenchymal progenitors distinct from satellite cells contribute to ectopic fat cell formation in skeletal muscle. *Nat Cell Biol*. 2010;12(2):143-152. https://doi.org/10.1038/ncb2014
37. Uezumi A, Ikemoto-Uezumi M, Zhou H, et al. Mesenchymal Bmp3b expression maintains skeletal muscle integrity and decreases in age-related sarcopenia. *J Clin Invest*. 2021;131(1):e139617. https://doi.org/10.1172/jci139617
38. Kanatani M, Sugimoto T, Nishiyama K, Chihara K. Stimulatory effect of insulin-like growth factor binding protein-5 on mouse osteoclast formation and osteoclastic bone-resorbing activity. *J Bone Miner Res*. 2000;15(5):902-910. https://doi.org/10.1359/jbmr.2000.15.5.902
39. Melville KM, Kelly NH, Khan SA, et al. Female mice lacking estrogen receptor-alpha in osteoblasts have compromised bone mass and strength. *J Bone Miner Res*. 2014;29(2):370-379. https://doi.org/10.1002/jbmr.2082
40. Yu M, Pal S, Paterson CW, et al. Ovariectomy induces bone loss via microbial-dependent trafficking of intestinal TNF+ T cells and Th17 cells. *J Clin Invest*. 2021;131(4):e143137. https://doi.org/10.1172/JCI143137
41. Imai Y, Youn MY, Inoue K, Takada I, Kouzmenko A, Kato S. Nuclear receptors in bone physiology and diseases. *Physiol Rev*. 2013;93(2):481-523. https://doi.org/10.1152/physrev.00008.2012
42. Yu W, Zhong L, Yao L, et al. Bone marrow adipogenic lineage precursors promote osteoclastogenesis in bone remodeling and pathologic bone loss. *J Clin Invest*. 2021;131(2):e140214. https://doi.org/10.1172/JCI140214
43. Ahlborg HG, Johnell O, Turner CH, Rannevik G, Karlsson MK. Bone loss and bone size after menopause. *N Engl J Med*. 2003;349(4):327-334. https://doi.org/10.1056/NEJMoa022464
44. Turner RT, Wakley GK, Hannon KS. Differential effects of androgens on cortical bone histomorphometry in gonadectomized male and female rats. *J Orthop Res*. 1990;8(4):612-617. https://doi.org/10.1002/jor.1100080418
45. Kurosawa T, Ikemoto-Uezumi M, Yoshimoto Y, et al. Tissue-specific functions of MSCs are linked to homeostatic muscle maintenance and alter with aging. *Aging Cell*. 2024;23(11):e14299. https://doi.org/10.1111/acel.14299
46. Sakai H, Uno H, Yamakawa H, et al. The androgen receptor in mesenchymal progenitors regulates skeletal muscle mass via Igf1 expression in male mice. *Proc Natl Acad Sci USA*. 2024;121(39):e2407768121. https://doi.org/10.1073/pnas.2407768121
47. Babey ME, Krause WC, Chen K, et al. A maternal brain hormone that builds bone. *Nature*. 2024;632(8024):357-365. https://doi.org/10.1038/s41586-024-07634-3

JBMR Plus, 2026, 10, ziaf178
https://doi.org/10.1093/jbmrpl/ziaf178
Research Article